Crossed beams studies of Mo($a\,^7S_3$) and Mo*($a\,^5S_2$) collisions with CH_4 and C_2H_6

Ryan Z. Hinrichs, Peter A. Willis, Hans U. Stauffer, Jonathan J. Schroden, and H. Floyd Davis[a)]
Department of Chemistry and Chemical Biology, Baker Laboratory, Cornell University, Ithaca, New York 14853-1301

(Received 1 October 1999; accepted 14 December 1999)

The interactions of Mo($a\,^7S_3$) and Mo*($a\,^5S_2$) with methane, CH_4, and ethane, C_2H_6, were studied under single collision conditions using the crossed molecular beams technique. Ground state Mo($a\,^7S_3$) atoms were found to be unreactive at all collision energies studied up to $\langle E_{\text{coll}}\rangle = 35.4$ kcal/mol. Nonreactive scattering of Mo($a\,^7S_3$) with methane and ethane was studied and compared to collisions with Ne and Ar. A forward peaking center-of-mass angular distribution, $T(\Theta)$, was necessary to simulate the elastic collisions with inert gases as well as inelastic collisions with the alkanes. At a collision energy of 14.4 kcal/mol with CH_4 and 21.0 kcal/mol with C_2H_6, inelastic collisions were found to transfer ~10% and ~19% of the initial kinetic energy into alkane internal energy, respectively. For collisions of Mo*($a\,^5S_2$)+CH_4, the dehydrogenation product, $MoCH_2$, was observed at all collision energies studied down to 2.1 kcal/mol. The reaction Mo*($a\,^5S_2$)+$C_2H_6 \rightarrow MoC_2H_4+H_2$ was observed down to $\langle E_{\text{coll}}\rangle = 4.5$ kcal/mol. For a given total energy (electronic+translational), it was found that electronic energy is highly effective in promoting this reaction whereas translational energy is ineffective. © *2000 American Institute of Physics.* [S0021-9606(00)00910-7]

I. INTRODUCTION

Saturated transition metal complexes are generally unreactive with alkanes under most conditions.[1] However, the insertion of coordinatively unsaturated transition metal centers (generated thermally or by photodissociation) into the C–H bonds of alkanes has been demonstrated in a number of select cases.[1,2] For example, Bergman and co-workers found that photolysis of the stable Cp*Rh$(CO)_2$ complex leads to CO loss producing Cp*RhCO, where Cp*=$C_5(CH_3)_5$. This 16 electron species inserts spontaneously into many alkanes, including CH_4, at room temperature.[3,4] Subsequently, these reactions have been studied in solution, the gas phase,[5] in liquefied noble gas solvents,[6] and by *ab initio* methods.[7] Interestingly, although the iridium and rhodium complexes were both found to be highly reactive, the analogous complex involving cobalt was not.[6] Calculations showed that the absence of reaction of the Co complex is likely due to a potential energy barrier for insertion of the triplet high-spin ground state into CH_4.[7] In the case of the Ir and Rh complexes, on the other hand, the ground states were found to be low spin singlets, having a negligible barrier for insertion.[7] Clearly, the combination of experiment and theory is making it possible to understand why certain transition metal complexes are highly reactive, whereas other closely related species are not.

In an effort to better understand the electronic factors controlling insertion of neutral *d*-electron centers into alkanes in the absence of ligand effects, reactions of transition metal atoms have been studied in low temperature matrices.[8–12] For example, transition metal atoms such as iron and copper have been cocondensed with methane in inert gas matrices at 15 K.[8–10] Most ground state atoms were found to be unreactive due to a large potential energy barrier for insertion. However, upon irradiation of the matrix using ultraviolet light, electronically excited atoms were found to insert spontaneously into the C–H bonds forming species such as $HFeCH_3$.[8] Infrared spectra of these C–H insertion intermediates were obtained, providing the first direct insight into the structure of the initially-formed complexes.

In the gas phase, a number of transition metal cations have been found to react efficiently with alkanes.[13,14] It is generally believed that C–H insertion is more favorable than C–C insertion because the spherical H atom can undergo multicenter bonding, effectively decreasing the energy at the transition state. Such interactions are less favorable for the highly directional sp^3 orbitals involved in the C–C bond in alkanes such as ethane, leading to higher C–C insertion barriers.[15] However, for transition metal cations, both C–H and C–C bond insertions have been observed in several systems.[16,17]

In some cases, it has been found that different electronic states of a given metal ion may react by different mechanisms, possibly resulting in different chemical products. For example, Armentrout and co-workers found that reactions of ground state $V^+(^5D)$ with HD lead to equal amounts of VH^+ and VD^+, indicating that the reaction involves an insertion mechanism.[18] Reactions of the excited triplet states of V^+, primarily the ^3F states, favor production of VH^+ over VD^+ by a factor of three, indicating a direct abstraction mechanism.[18] For reactions with CH_4 and C_2H_6, $Fe^+(^4F)$ and $Fe^+(^6D)$ both react by a direct abstraction mechanism,[16]

[a)]Electronic mail: HFD1@cornell.edu

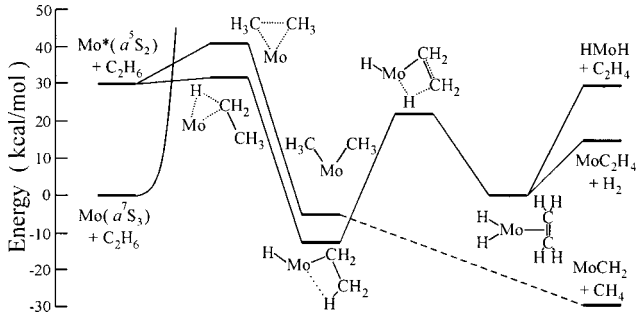

FIG. 1. Reaction energetics for $Mo+C_2H_6$. See text for details.

whereas reactions of Sc^+ and V^+ are initiated by C–H insertion.[17,19,20]

More recently, gas phase studies have been extended to reactions of neutral transition metal atoms in flow tube reactors.[21–24] The rates of bimolecular reactions were inferred by monitoring the consumption of the transition metal atoms as a function of hydrocarbon partial pressure.[25,26] For example, metastable $V^*(3d^4 4s^1, a\,^4D)$ atoms, prepared by stimulated emission pumping (SEP), were found to be deactivated at essentially the gas kinetic limit by collisions with ethylene.[25] In experiments using the alkanes CH_4 and C_2H_6, on the other hand, it was found that deactivation was less efficient, occurring in only 1 in 75 and 1 in 25 hard sphere collisions, respectively.[25] The metastable low spin $Mo^*(4d^5 5s^1, a\,^5S_2)$ state was observed to be deactivated on essentially every hard sphere collision with CH_4 and C_2H_6.[26] However, because products of the deactivation process were not detected, the relative importance of chemical reaction vs. electronic quenching was not determined.

The chemical products from metastable $Mo^*(^5S_2) + CH_4$ reactions under single collision conditions were first directly observed in our laboratory.[27] The $MoCH_2$ dehydrogenation products were detected at collision energies of 7.2 and 13.0 kcal/mol. No dehydrogenation products were observed for ground state $Mo(4d^5 5s^1, a\,^7S_3) + CH_4$ at collision energies up to 20.2 kcal/mol.[27]

Siegbahn *et al.* have calculated several minima and saddle points lying on the potential surfaces for the interactions of Mo with CH_4 and C_2H_6.[22] A schematic reaction coordinate for the $Mo+C_2H_6$ system is shown in Fig. 1. All stationary points shown in Fig. 1 are based on *ab initio* calculations,[22,28] thermodynamic data from the literature,[29] and results from the present experiments. The calculated C–H and C–C insertion barriers lie 37.8 and 41.2 kcal/mol, respectively, above the $Mo(^7S_3)+C_2H_6$ reactant asymptote [7.0 and 10.4 kcal/mol, respectively, above $Mo^*(^5S_2) + C_2H_6$ reactants], although the C–H insertion barrier is drawn lower in Fig. 1 based on experiments reported here.[30] The energetics of the $HMoC_2H_5$ intermediate and $H_2MoC_2H_4$ resulting from β-hydrogen migration were derived from the results of an earlier *ab initio* study.[28]

Three possible product channels are shown in Fig. 1 for the reaction of $Mo+C_2H_6$. The most exoergic channel, based on *ab initio* calculations, is formation of $MoCH_2+CH_4$ following C–C bond insertion.[22] However, the energetics of the reaction intermediates following formation of CH_3MoCH_3 have not been calculated. Insertion into the C–H bond of C_2H_6 can lead to dehydrogenation, forming $MoC_2H_4+H_2$, or to ethylene elimination producing $MoH_2+C_2H_4$.[31,32]

Calculations indicate that all stationary points along the reaction coordinate (other than the ground state reactants) in Fig. 1 are of quintet spin multiplicity.[22,28] Thus, a spin–flip must occur in order for the $Mo(^7S_3)$ state to react. One of the goals of this work is to experimentally determine whether or not this spin-forbidden process plays an important role.

Recent studies in our laboratory revealed that the potential energy barrier for C–H insertion of ground state $Y(4d^1 5s^2, a^2D_{3/2})$ atoms into C_2H_6 is 19.9 ± 3.0 kcal/mol.[33] At collision energies above this barrier, production of $YH_2+C_2H_4$ is dominant, but a second channel leads to formation of $YC_2H_4+H_2$.[33] The ground state $Y(a\,^2D_J)+C_2H_6$ diabatic surfaces are strongly repulsive due to the d^1s^2 character of ground state Y. The large adiabatic barrier for C–H insertion results from an avoided crossing between these surfaces and attractive surfaces, also of doublet multiplicity, correlating to the ground state C–H insertion intermediate.[22] In this case, both the Y atom reactants and the calculated ground state insertion intermediates are of doublet multiplicities, and translational energy is relatively efficient in promoting reaction.

This study is an expansion of our previous work on the collisions of ground state $Mo(^7S_3)$ and electronically excited $Mo^*(^5S_2)$ atoms with the simplest hydrocarbon, CH_4.[27] In the present work, the signal-to-noise ratio has been improved through the use of 157 nm photoionization of reactive and nonreactive products (rather than electron impact ionization). We have also carried out studies of $Mo^*(^5S_2)+C_2H_6$ reactions as well as nonreactive collisions of $Mo(^7S_3)$ atoms with CH_4 and C_2H_6. These nonreactive collisions are compared to elastic collisions of $Mo(^7S_3)$ with inert gas atoms such as Ne and Ar.

II. EXPERIMENT

All experiments reported here were performed using a rotatable source crossed molecular beams apparatus, which has been described in detail elsewhere.[34] The Mo atoms were generated by laser ablation (532 nm, 20 mJ/pulse) from a 0.25 in. diameter molybdenum rod (Alfa Aesar, 99%) and subsequently entrained in a supersonic expansion of an inert carrier gas. The metal beam was skimmed and collimated by a set of defining slits to an angular full width at half maximum (FWHM) of 2.5°. The populations of atomic electronic states in the Mo beam were characterized by laser induced fluorescence (LIF) excitation spectroscopy at the interaction region. The frequency doubled output of a Nd:YAG (Continuum 9030) pumped dye laser (Scanmate 2E, Pyridine 1) was scanned over a wavelength range containing transitions associated with the ground electronic state, $Mo(^7S_3)$, as well as several transitions from the low-lying electronically excited $Mo^*(^5s_2)$ and $Mo(^5D_J)$ states. Fluorescence signal was collected by optics perpendicular to the atomic and laser beams and focused onto a photomultiplier tube (PMT). Fluorescence signal was only observed for transitions out of the ground $Mo(^7S_3)$ state.

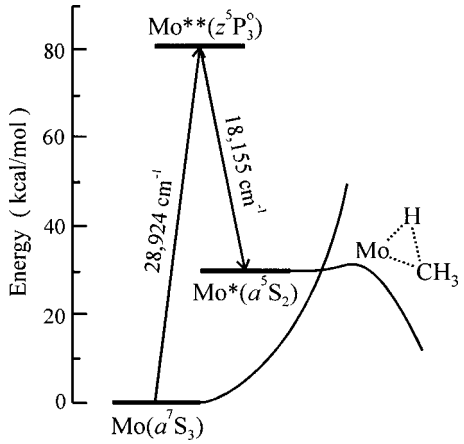

FIG. 2. Optical pumping scheme for production of metastable electronically excited Mo*($a\ ^5S_2$) atoms.

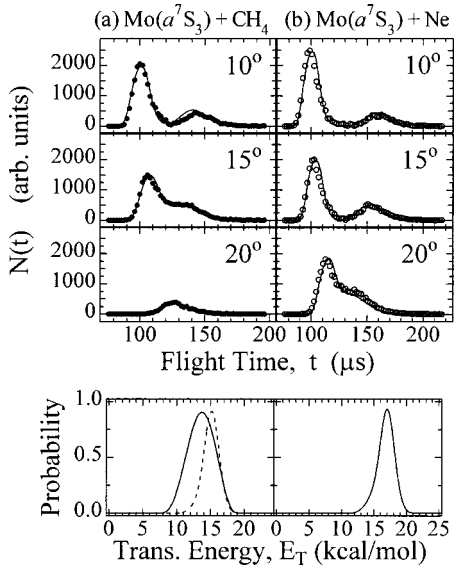

FIG. 3. Nonreactively scattered Mo($a\ ^7S_3$) TOF spectra for (a) Mo($a\ ^7S_3$) + CH_4 at $\langle E_{coll}\rangle = 14.4$ kcal/mol and (b) Mo($a\ ^7S_3$) + Ne at $\langle E_{coll}\rangle = 16.8$ kcal/mol. Bottom (a): Best-fit $P(E_T)$ (solid line) and collision energy distribution. Bottom (b): Collision energy distribution used as $P(E_T)$ for elastic collisions.

The doubled output of a second Nd:YAG (Continuum 9030) pumped dye laser (Scanmate2E or FL3002) was used in experiments in which it was necessary to transfer population to the metastable excited Mo*($^5S_2$) state, lying 10 768 cm^{-1} above the ground state.[30] The laser was expanded using an optical telescope to ~1.2 cm diameter and crossed the Mo beam 8 mm upstream of the interaction region. As depicted in Fig. 2, the Mo atoms are excited on the spin-forbidden Mo**($^5P^0_3$)←Mo($^7S_3$) transition at 345.738 nm. Following excitation, the Mo**($^5P^0_3$) state radiatively decays to the desired Mo*($^5S_2$) state, a fully allowed transition, at 550.802 nm with an Einstein A coefficient of $3.0 \times 10^8\ s^{-1}$.[35] Although decay to the $^5D_4$ state also occurs, as discussed in Section IV B, this state is known to be relatively unreactive from previous experiments[26] and is only populated to a very small extent in these experiments.[35]

A skimmed molecular beam, directed at right angles to the metal beam, has an angular FWHM of 5.0°. Scattered species from collisions at the interaction region are detected by a fixed triply-differentially pumped mass spectrometer with an angular resolution of 1.5°. Recoiling neutral fragments are ionized by 157 nm photons generated by an F_2 excimer laser (Lambda Physik LPX220i). Once ionized, the species are mass selected by a quadrupole mass filter and detected by a channeltron ion detector. Positive ions are unable to enter the detector because the front lenses are biased at +100 V. Negative ions, if present, strike the ion lens assembly and are lost. Experiments were also carried out in which positive metal ions produced in the ablation process were extracted from the beam in the differential pumping region, prior to entering the main scattering chamber. No difference in signal was seen with the extraction field ''on'' and ''off,'' indicating that none of the observed signal results from reactions of ionic species leading to neutral metallic products. The isotopic abundances of Mo are ^{92}Mo:15%, ^{94}Mo:9%, ^{95}Mo:16%, ^{96}Mo:17%, ^{97}Mo:9.5%, ^{98}Mo:24%, and ^{100}Mo:9.5%.[36] All studies described here, unless otherwise noted, were recorded using the most abundant isotope, ^{98}Mo. The experimental data were analyzed using a forward convolution program described in previous publications.[37,38]

III. RESULTS AND ANALYSIS

A. Collisions of Mo($^7S_3$) with alkanes

The collisions of Mo($^7S_3$) + CH_4 were studied at $\langle E_{coll}\rangle = 4.7$ and 14.4 kcal/mol. No reactive signal was observed for ground state Mo($^7S_3$) atoms colliding with CH_4 at these collision energies. However, nonreactively scattered Mo($^7S_3$) atoms were detected at laboratory angles ranging from 5° to 35°. Time-of-flight (TOF) spectra taken at Mo^+ ($m/e = 98$) at $\langle E_{coll}\rangle = 14.4$ kcal/mol are shown in Fig. 3(a). The solid lines represent best-fit simulations, which will be discussed below. The TOF spectra recorded at $\langle E_{coll}\rangle = 4.7$ kcal/mol were qualitatively similar to the spectra shown here.

In order to better understand this nonreactive scattering process, additional experiments were performed using inert gas colliding partners. Elastic scattering of Mo($^7S_3$) + Ne was studied at $\langle E_{coll}\rangle = 5.0$ and 16.8 kcal/mol, and Mo($^7S_3$) + Ar was studied at 21.4 kcal/mol. TOF spectra for Mo($^7S_3$) + Ne scattering at 16.8 kcal/mol are shown in Fig. 3(b). The solid lines were generated using the forward convolution analysis program. The TOF spectra and laboratory angular distributions are simulated from input center-of-mass (c.m.) translational, $P(E_T)$, and angular, $T(\Theta)$, distributions, which are assumed to be separable. Since Mo($^7S_3$) + Ne collisions are elastic, the $P(E_T)$ used to simulate the data, shown at the bottom of Fig. 3(b), has been assumed to be identical to the collision energy distribution, based on the measured reactant beam velocities. Figure 4 shows the laboratory angular distribution for Mo($^7S_3$) elastically scattered from Ar. The solid line shown in the lab angular distribution is a simulation using the collision energy distribution as $P(E_T)$ and the $T(\Theta)$ shown in Fig. 4. This elastic $T(\Theta)$ obtained from the Mo($^7S_3$) + Ar fits was also used to generate the best-fit Mo($^7S_3$) + Ne TOFs.

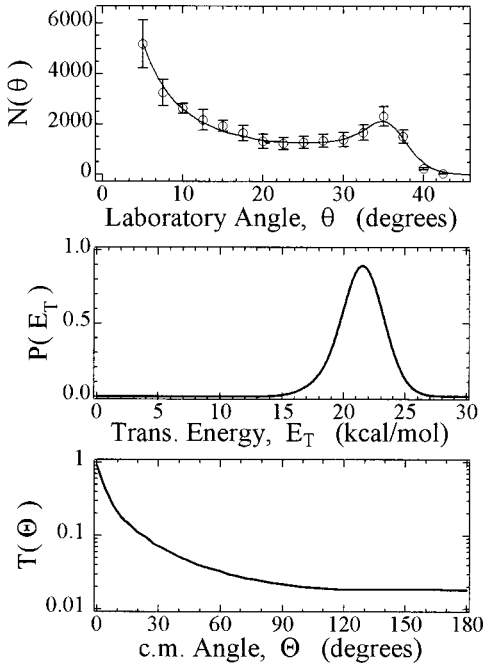

FIG. 4. Laboratory angular distribution (error bars are 1 σ of 3 replicate measurements) for elastic scattering of Mo($^7S_3$)+Ar at $\langle E_{\text{coll}}\rangle$ = 21.4 kcal/mol. Solid line is best fit generated using c.m. collision energy distribution, $P(E_T)$, and best-fit angular distribution, $T(\Theta)$ (semilog plot).

The best-fit simulations for the Mo($^7S_3$)+CH_4 nonreactive TOF spectra [Fig. 3(a)] were also generated using the $T(\Theta)$ obtained from the elastic collisions. The $P(E_T)$ used for these simulations is shown as a solid line in the bottom portion of Fig. 3(a) and for comparison the collision energy distribution is shown as a dashed line. On average, Mo($^7S_3$)+CH_4 collisions transfer ~10% of the initial kinetic energy into internal energy of the recoiling CH_4 molecule.

The collisions of Mo($^7S_3$)+C_2H_6 were studied at $\langle E_{\text{coll}}\rangle$ = 21.0 and 35.4 kcal/mol. Figure 5 shows a Newton diagram in velocity space for collisions of Mo+C_2H_6 at $\langle E_{\text{coll}}\rangle$ = 21.0 kcal/mol. Although calculations predict that

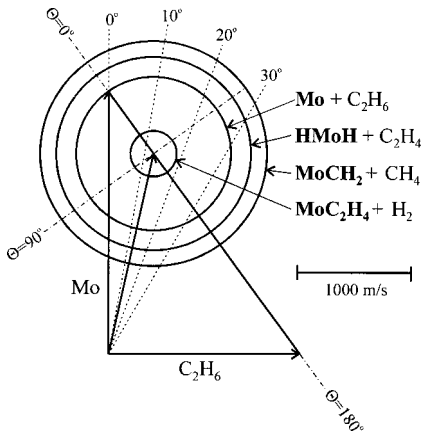

FIG. 5. Newton diagram for collisions of Mo+C_2H_6 at $\langle E_{\text{coll}}\rangle$ = 21.0 kcal/mol. All product Newton spheres are based on calculated energetics. Note that reactive energetics are relative to Mo*($^5S_2$) state and nonreactive sphere is for elastic (i.e., not super-elastic) scattering.

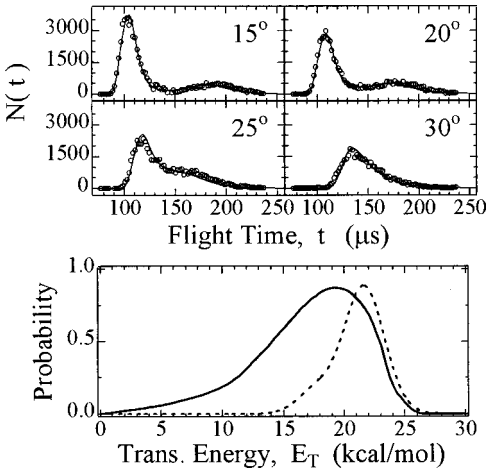

FIG. 6. Nonreactively scattered Mo($^7S_3$) TOF spectra for collisions with C_2H_6 at $\langle E_{\text{coll}}\rangle$ = 21.0 kcal/mol. Solid line simulations generated using $T(\Theta)$ in Fig. 4 and $P(E_T)$ shown at bottom of this figure (solid line). Dashed line represents collision energy distribution.

several product channels are energetically accessible at these collision energies,[22] no reactive product signal was observed. However, nonreactively scattered Mo($^7S_3$) atoms were observed and representative TOFs are shown in Fig. 6 for $\langle E_{\text{coll}}\rangle$ = 21.0 kcal/mol. The solid line fits were generated using the elastic $T(\Theta)$ from Mo($^7S_3$)+Ar and the $P(E_T)$ shown at the bottom of Fig. 6. Also shown as a dashed line in Fig. 6 is the collision energy distribution. On average, Mo($^7S_3$)+C_2H_6 collisions were found to be more inelastic than Mo($^7S_3$)+CH_4 collisions, with ~19% of the initial kinetic energy converted into internal energy of the recoiling C_2H_6 molecule.

B. Collisions of Mo*($^5S_2$) with methane, CH_4

The collisions of metastable electronically excited Mo*($^5S_2$) atoms with CH_4 have also been studied at the collision energies noted in Table I. Two distinct effects are observed when the pump laser is turned on to prepare Mo*($^5S_2$) upstream of the collision volume. First, reactive signal associated with dehydrogenation products, $^{98}MoCH_2+H_2$, is clearly observed at all collision energies studied. As expected, when the pump laser is tuned slightly off the ($^5P_3^0 \leftarrow {}^7S_3$) resonance, the $MoCH_2$ signal disappears. We have previously reported the observation of this reactive signal at $\langle E_{\text{coll}}\rangle$ = 7.2 and 13.0 kcal/mol.[27] In our previous study, the $MoCH_2$ products were ionized for mass analysis using electron impact ionization. In this current study, we have revisited this system using 157 nm photoionization of the $MoCH_2$ products and nonreactively scattered Mo atoms.

The increased sensitivity of photoionization compared to electron impact ionization allows us to obtain improved signal-to-noise ratios. This is particularly valuable at lower collision energies where beam intensities are reduced. The TOF spectra for the $MoCH_2$ products at $\langle E_{\text{coll}}\rangle$ = 4.7 kcal/mol are shown in Fig. 7. The solid lines represent the best-fit simulations generated using the $P(E_T)$ and $T(\Theta)$ shown in Fig. 8. Dashed lines shown in the $P(E_T)$ represent the limit of kinetic energy release distributions which satisfactorily fit

TABLE I. Experimental conditions for Mo+alkane collisions.

	Molybdenum beam				Secondary beam		
	$\langle E_{coll}\rangle$[a]	Cond	v_{pk}[b]	FWHM	Cond	v_{pk}[b]	FWHM
Mo+CH_4	2.1	Ar	905	95	25% in Ar	696	118
	4.7	Ne	1284	130	Pure	1110	230
	14.4	He	2426	298	20% in H_2	1762	190
Mo+CD_4	5.0	Ne	1270	130	Pure	980	300
Mo+C_2H_6	4.5	Ar	905	95	Pure	888	176
	6.8	Ne	1316	156	Pure	888	176
	21.0	He	2478	294	20% in H_2	1404	130
	35.4	H_2	3244	444	10% in H_2	1628	144
Mo+Ne	5.0	Ne	1270	130	Pure	980	200
	16.8	He	2450	260	20% in H_2	1628	144
Mo+Ar	21.4	He	2306	254	20% in H_2	1064	104

[a]$\langle E_{coll}\rangle$ in kcal/mol.
[b]Velocities in m/s.

the laboratory angular distribution (not shown). The shaded portion on the $T(\Theta)$ represents our uncertainty in the degree of forward–backward symmetry. It has been determined that $T(\Theta=0°)/T(\Theta=180°)=0.97\pm0.12$, implying an essentially forward–backward symmetric $T(\Theta)$. Qualitatively similar c.m. distributions have been obtained at the higher collision energies studied. The $MoCH_2$ signal has also been observed at the center-of-mass angle, θ_{cm}, for $\langle E_{coll}\rangle = 2.1$ kcal/mol; however, a complete data set was not recorded due to the extremely weak signal resulting from the low Mo beam intensity using Ar carrier gas.

We have also studied this reaction using deuterated methane, CD_4, at $\langle E_{coll}\rangle = 5.0$ kcal/mol. The laboratory angular distribution for the $MoCD_2$ products is shown in Fig. 9. The c.m. distributions used to simulate these data are shown at the bottom of Fig. 9. Dashed lines in the lab angular distribution have been generated using the best-fit $T(\Theta)$ and the dashed line $P(E_T)$s. The heavier recoil partner (D_2 instead of H_2) increases our sensitivity to the exact form of the $T(\Theta)$. The shaded region indicates our uncertainty in the depth of the $T(\Theta)$, i.e., comparing $T(\Theta=0°)$ to $T(\Theta=90°)$. For the best-fit distribution $T(\Theta=0°)/T(\Theta=90°)=2.2$, while a range of ±0.8 still generates acceptable fits.

The second effect observed when the pump laser is turned on is illustrated in the ^{98}Mo TOF spectrum recorded at $\theta=15°$ in Fig. 10. The open circles show the data with the pump laser off while the filled circles show the result of turning the pump laser on. The integrated product signal intensity decreases by approximately 35% while the shape of each TOF spectrum remains unchanged. Similar behavior is observed at all other laboratory angles.

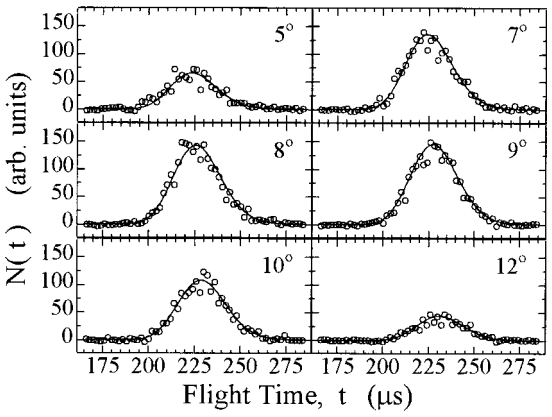

FIG. 7. TOF spectra for $MoCH_2$ products from Mo*($^5S_2$)+CH_4 collisions at $\langle E_{coll}\rangle = 4.7$ kcal/mol.

C. Collisions of Mo*($^5S_2$) with ethane, C_2H_6

For the case of Mo*($^5S_2$)+C_2H_6, the MoC_2H_4 dehydrogenation products were observed at all collision energies studied, ranging from 4.5 to 35.4 kcal/mol. The laboratory angular distribution for MoC_2H_4 products at $\langle E_{coll}\rangle = 21.0$ kcal/mol is shown in Fig. 11. Due to the light mass of the recoiling H_2 counterfragment, the laboratory angular distribution is peaked at θ_{cm} and falls off sharply on either side. The solid line simulation was generated using the best-fit c.m. distributions also shown in Fig. 11. These c.m. distributions are very similar to those obtained for the Mo*($^5S_2$) +CH_4 products with a $P(E_T)$ peaking very close to zero kinetic energy. At $\langle E_{coll}\rangle = 21.0$ kcal/mol, the $P(E_T)$ peaks at 2.5 kcal/mol, whereas at the lower collision energy of 6.8

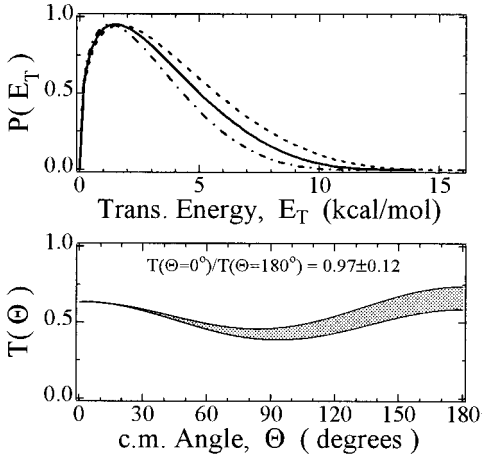

FIG. 8. Best-fit c.m. distributions (solid lines), $P(E_T)$, and $T(\Theta)$, for Mo*($^5S_2$)+CH_4→$MoCH_2$+H_2 at $\langle E_{coll}\rangle = 4.7$ kcal/mol. Dashed lines shown in the $P(E_T)$ correspond to limits of acceptable fits. Shaded region shows uncertainty in forward–backward symmetry in $T(\Theta)$.

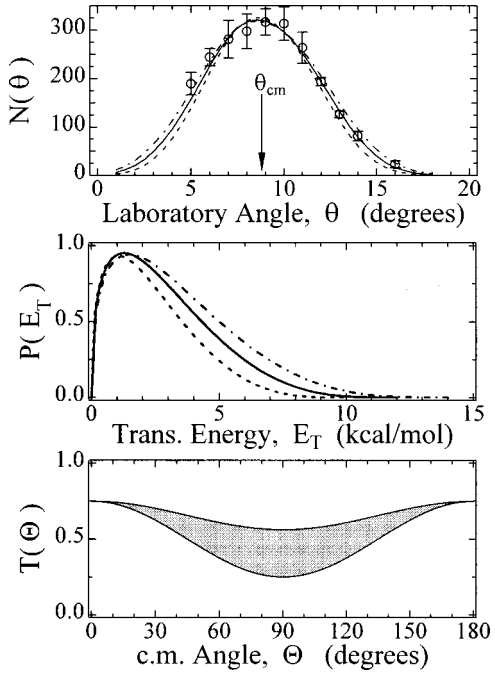

FIG. 9. Lab angular distribution and best fit c.m. distributions for the reaction $Mo^*(^5S_2)+CD_4 \rightarrow MoCD_2+D_2$ at $\langle E_{coll}\rangle = 5.0$ kcal/mol. Dashed lines shown in the $P(E_T)$ correspond to limits of acceptable fits. Shaded region shows uncertainty in depth of $T(\Theta)$.

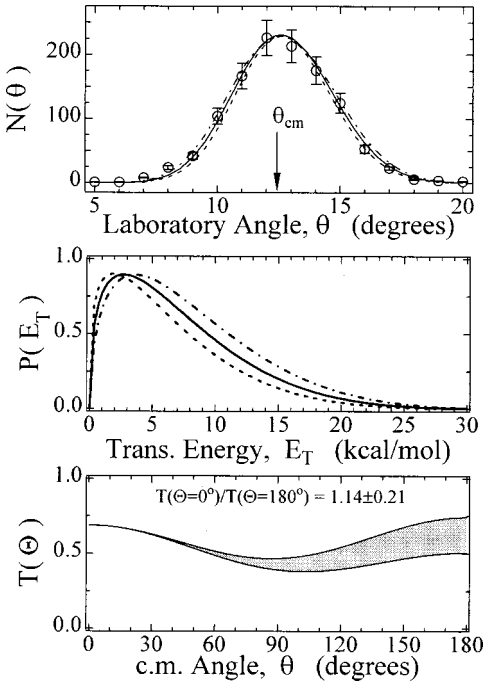

FIG. 11. Lab angular distribution and best fit c.m. distributions for the reaction $Mo^*(^5S_2)+C_2H_6 \rightarrow MoC_2H_4+H_2$ at $\langle E_{coll}\rangle = 21.0$ kcal/mol. Dashed lines shown in the $P(E_T)$ correspond to limits of acceptable fits. Shaded region shows uncertainty in forward–backward symmetry in $T(\Theta)$.

kcal/mol, the peak is near 1.3 kcal/mol. The $T(\Theta)$ was found to be essentially forward–backward symmetric, with $T(\Theta = 0°)/T(\Theta = 180°) = 1.14 \pm 0.21$.

Shown in Fig. 12 are the MoC_2H_4 TOF spectra taken at the center-of-mass angles for $\langle E_{coll}\rangle = 35.4$ kcal/mol($\theta_{cm} = 10°$) with the pump laser off and $\langle E_{coll}\rangle = 4.5$ kcal/mol($\theta_{cm} = 15°$) with the pump laser turned on. The excited $Mo^*(^5S_2)$ state lies 10 768 cm^{-1} (30.8 kcal/mol) above the $Mo(^7S_3)$ ground state.[30] Thus the total energy ($E_{kinetic} + E_{electronic}$) is approximately equal for these two experiments. The top portion of Fig. 12 shows the two collision energy distributions with the $\langle E_{coll}\rangle = 4.5$ kcal/mol shifted by the electronic energy of the $Mo^*(^5S_2)$ state. No signal was observed when the total available energy was in translation, whereas reactive signal could be easily observed for electronically excited $Mo^*(^5S_2)$. It should be noted that the maximum accessible Newton spheres for recoiling MoC_2H_4 products are similar for both conditions since they depend mainly on the total available energy (which is essentially identical for both cases), and the reduced mass of the product fragments.

Observation of $^{98}MoH_2$ signal is complicated by the presence of ^{100}Mo(^{98}Mo:24.1%, ^{100}Mo:9.6%). After an extensive search at $m/e = 98$, 100, and 102, at a number of laboratory angles and collision energies, we conclude that no MoH_2 signal is observed above the background signal. As indicated in Fig. 1, a third possible product channel may result from initial C–C bond insertion forming CH_3MoCH_3, followed by production of $MoCH_2+CH_4$. The Newton diagram (Fig. 5) for $Mo^*(^5S_2)+C_2H_6$ collisions at $\langle E_{coll}\rangle$

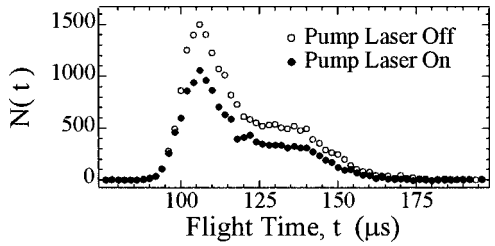

FIG. 10. TOF spectra for nonreactively scattered Mo atoms from CH_4 recorded at $\theta = 15°$. The total signal intensity is decreased by ~35% when the pump laser is turned on.

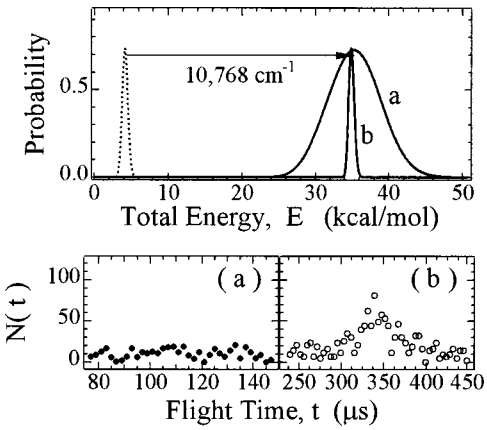

FIG. 12. Top: Collision energy distributions for $Mo+C_2H_6$ for (a) ground state $Mo(^7S_3)+C_2H_6$ at $\langle E_{coll}\rangle = 35.4$ kcal/mol, and (b) $\langle E_{coll}\rangle = 4.5$ kcal/mol distribution shifted by the excitation energy to the $Mo^*(a\ ^5S_2)$ state. Bottom: MoC_2H_4 TOF spectra recorded at the angle of the center-of-mass, θ_{cm}, for (a) $Mo(^7S_3)+C_2H_6$ at $\langle E_{coll}\rangle = 35.4$ kcal/mol, and (b) $Mo^*(^5S_2)+C_2H_6$ at $\langle E_{coll}\rangle = 4.5$ kcal/mol.

$=21.0$ kcal/mol demonstrates that the maximum Newton spheres for $MoCH_2$ products (as well as MoH_2 products) are larger than for MoC_2H_4. This provides the opportunity to search for these products outside the range where fragmentation of MoC_2H_4 might contribute to the background signal. However, even after extensive averaging at $m/e=112(MoCH_2^+)$ at a number of laboratory angles at several different collision energies, no evidence for this channel was observed from $Mo^*(^5S_2)+C_2H_6$.

IV. DISCUSSION

A. Collisions of $Mo(^7S_3)+CH_4,C_2H_6$

Distinct similarities are observed in the TOF spectra and $T(\Theta)$ for collisions of $Mo(^7S_3)$ with CH_4 and Ne. In this comparison, it is informative to consider an analogous pair of systems, Ar+Ne and $Ar+CH_4$. For both elastic scattering of Ar+Ne (Ref. 39) and inelastic scattering of $Ar+CH_4$,[40] rainbow and supernumerary rainbow scattering has been observed in crossed beams studies. This has allowed for the determination of well depths for the interactions of these two systems. Ar+Ne is bound by ~ 50 cm^{-1} whereas $Ar+CH_4$ has a well depth of ~ 120 cm^{-1}.[39,40] In addition to the slightly deeper well, $Ar+CH_4$ collisions are inelastic and modeling the potential energy surface (PES) requires the inclusion of an anisotropic term related to the ability of Ar to impose a torque on CH_4 during the scattering process.[40]

In our studies of $Mo(^7S_3)+Ne/Ar$ and $Mo(^7S_3)+CH_4/C_2H_6$, no evidence for rainbow scattering was observed due to the high collision energies and lower experimental angular resolution compared to the Ar scattering studies.[39,40] However, the use of the same $T(\Theta)$ for inert gas and alkane scattering implies that the dynamics of the scattering events are qualitatively similar. The ground state $Mo(^7S_3)+$alkane collisions are dominated by the repulsive part of the PES with negligible contribution from complex formation. This situation contrasts that seen recently in our studies of second row transition metal atoms with unsaturated hydrocarbons such as alkenes and alkynes.[37,38] In those cases, the strong peaking of the $T(\Theta)$ near $\Theta=180°$ and the subsequently determined forward–backward symmetry for the nonreactively scattered ground state atoms was taken as evidence for the formation of collision complexes having lifetimes exceeding their picosecond rotational timescales.[37,38] Metal–alkene and metal–alkyne π-complexes are typically bound by 30–50 kcal/mol relative to the separated reactants.[22] In the case of $Mo(^7S_3)+CH_4$ and $Mo(^7S_3)+C_2H_6$, in the absence of C–H insertion, the attractive interaction is expected to be comparable in magnitude to that with inert gas atoms, having binding energies with transition metal atoms typically in the range of 100–350 cm^{-1} (0.3–1.0 kcal/mol).[41]

B. Reactivity of $Mo^*(^5S_2)$ state

Excited state $Mo^*(^5S_2)$ atoms were found to react efficiently with CH_4 and C_2H_6 to produce $MoCH_2+H_2$ and $MoC_2H_4+H_2$, respectively. We have observed these dehydrogenation products at all collision energies studied, down to 2.1 kcal/mol for $Mo^*(^5S_2)+CH_4$. At this collision energy, the total energy available to promote the observed dehydrogenation reaction is the sum of the translational and electronic energy, 32.9 kcal/mol. This sets a strict upper limit of 32.9 kcal/mol relative to ground state $Mo(^7S_3)$ (i.e., 2.1 kcal/mol above $Mo^*(^5S_2)$) for all barriers along the quintet reaction coordinate to form $MoCH_2+H_2$.

A previous theoretical study has calculated the transition state for C–H insertion to lie on the quintet PES 37.8 kcal/mol above the ground state reactants.[22] This is 7.0 kcal/mol above the energy of separated $Mo^*(^5S_2)+CH_4$, suggesting that an adiabatic insertion barrier may exist for the electronically excited $Mo^*(^5S_2)$ state. From our experimental observations, if such a barrier above $Mo^*(^5S_2)+CH_4$ exits, it must be less than 2.1 kcal/mol above the quintet reactant asymptote. Although the $Mo+CH_4$ calculations did not address the origin of this barrier, Li and Balasubramanian have carried out detailed calculations on the insertion of various electronic states of Mo into H_2.[31] It was found that ground state $Mo(^7S_3)$ atoms have to surmount an 89.5 kcal/mol barrier for insertion. A barrier of 28 kcal/mol was calculated for insertion of the electronically excited $Mo^*(^5S_2)$ state.[31] However, the $Mo(b\,^5D)$ state, lying 57 kcal/mol above the ground state, was calculated to insert spontaneously into H_2 forming ground state $MoH_2(^5B_2)$.[31] This suggests that the adiabatic barrier for insertion of $Mo^*(^5S_2)$ is associated with an avoided crossing of diabatic curves correlating to $Mo^*(^5S_2)$ and $Mo(b\,^5D)$.

Weisshaar *et al.* have measured the rate for depletion of $Mo^*(^5S_2)$ atoms in the presence of CH_4 at room temperature to be $k_1=(3-4)\times 10^{-10}\,cm^3\cdot s^{-1}$.[26] This depletion rate is near the gas kinetic limit for collisions of $Mo^*(^5S_2)$ with CH_4. If the depletion is due to reactivity rather than electronic quenching, then the true insertion barrier must lie at most a fraction of a kcal/mol above the $Mo^*(^5S_2)+CH_4$ reactants.[26] The depletion of the metastable $Mo(a\,^5D_J)$ was also measured as 5–10 times less efficient compared to the $Mo^*(^5S_2)$ state.[26] If we assume that the difference in depletion rates for these two metastable states is proportional to their reactivity, using the known branching fraction for decay into the metastable $(a\,^5D_J)$ state,[35] the maximum contribution from reactions of the $Mo(a\,^5D_J)$ states to form $MoCH_2$ products in our experiment is 4%.

We expect that elimination of molecular hydrogen from the $HMoCH_3$ intermediate involves a stepwise process.[27,42] Following insertion, this process involves migration of an α-hydrogen to form a second stable intermediate, H_2MoCH_2, which subsequently decays to products. The best-fit $P(E_T)$ for the 4.7 kcal/mol data set peaks near $E_T=1$ kcal/mol for a total available energy of 10 kcal/mol.[22] Thus, as the H_2MoCH_2 intermediate eliminates H_2, most of the available energy is channeled into vibrational modes perpendicular to the reaction coordinate. Due to the small reduced mass of the recoiling products, only a relatively small fraction of the total angular momentum, **J**, can become relative orbital angular momentum in the products, $\mathbf{L}'$. Thus, conservation of angular momentum may channel a significant amount of rotational energy of the complex into product rotation, leading to an angular distribution peaking less sharply at the poles than in our recent studies of reactions involving elimination

of ethylene[33] and carbon monoxide[43] from long-lived intermediates.

In the case of $Mo^*(^5S_2)+C_2H_6$ reactions, dehydrogenation products were observed at the lowest collision energy studied, $\langle E_{coll}\rangle = 4.5$ kcal/mol, placing an upper limit of 35.3 kcal/mol above $Mo(^7S_3)+C_2H_6$ for any barrier along the reaction coordinate. To date, it has been assumed that the C–H activation barrier for C_2H_6 is energetically similar to that for CH_4 activation. Indeed, Weisshaar *et al.* have found the depletion rate of $Mo^*(^5S_2)$ in the presence of C_2H_6 to be very similar to that measured for CH_4.[26]

The calculated height of the β-hydrogen migration transition state for $Mo^*(^5S_2)+C_2H_6$ is found to lie energetically below the C–H insertion barrier.[22,28] For transition metals containing unoccupied *d*-orbitals, these β-migration transition state structures may be further stabilized by intramolecular β-agostic interactions.[44] It is possible that at higher levels of theory these β-agostic interactions may become evident for the $Mo+C_2H_6$ system, further lowering the height of this migration barrier.

C. Effect on nonreactive scattering by laser excitation

The intensity of the nonreactively scattered Mo atoms is found to decrease by $\sim 35\%$ when optical pumping to populate the $Mo^*(^5S_2)$ state is performed upstream of the interaction volume. However, the shapes of the TOF spectra remain unchanged. The absence of an increase in nonreactively scattered Mo atoms arriving at short flight times when the laser is turned on indicates that ''superelastic'' scattering involving transfer of electronic energy to translational energy is negligible. As noted above, ground state $Mo(^7S_3)$ atoms do not insert into the C–H bond of CH_4 and C_2H_6. The fact that no increase in wide angle nonreactive signal peaking near $\Theta = 180°$ is seen when the laser is turned on indicates that insertion of excited state atoms followed by decay back to reactants must be a negligible process. If we assume that the densities of states are comparable for both the C–H insertion and the α-hydrogen migration transition states, then the relative heights of these barriers determine the fraction of intermediates that will reform reactants. Since we see no evidence for decay of insertion complexes back to reactants, we believe that the C–H insertion barrier is higher than any subsequent barriers for reaction. Vibrational frequencies and moments of inertia, not presently available, are necessary to better quantify the relative energies of these two barriers.

The primary origin of the decrease in wide angle nonreactive Mo signal upon turning on the laser is that a significant fraction of the excited $Mo^*(^5S_2)$ atoms undergo reaction producing $MoCH_2+H_2$. Such atoms are no longer available to undergo inelastic nonreactive scattering, decreasing the signal from this channel. By comparing the fractional decrease in wide-angle nonreactive scattering (typically 35%) to the fractional decrease in the population of ground state $Mo(^7S_3)$ atoms in the beam (using LIF), we attempted to determine the fraction of excited state atoms undergoing reaction. Unfortunately, this measurement is complicated by the fact that the $z\,^5P_3^0$ state used in our pumping scheme lies slightly more than halfway to the ionization continuum for Mo.[30] Consequently, $1+1$ resonance enhanced multiphoton ionization (REMPI) prior to collision was also found to contribute to the decreased wide-angle nonreactive scattering of Mo atoms, because positive ions cannot enter the detector. At low laser powers (0.1 mJ, 1.2 cm dia.), this process could be minimized, but not completely eliminated, so it is not possible to accurately determine the exact fraction of excited state $Mo^*(^5S_2)$ undergoing reaction. However, we reiterate that experiments using strong electric fields at the interaction region had no effect on the measured TOF spectra recorded for $MoCH_2$, MoC_2H_4, or Mo from nonreactive elastic and inelastic collisions. This indicates that the observed signals result exclusively from collisions of neutral transition metal atoms, with no contributions from events involving Mo^+.

D. Comparison of ground and excited state reactivity

The $Mo^*(^5S_2)$ state reacts efficiently with methane and ethane, while the ground $Mo(^7S_3)$ state has been found to be unreactive at all collision energies studied. Since both electronic states considered have a $4d^5(a\,^6S)5s^1$ configuration, the only difference is in the alignment of the spin of the $5s^1$ electron. It is well known that low-spin states insert more readily into H–H, C–H, and C–C bonds.[22,31] The availability of spin-paired electrons facilitates $s-d$ hybridization and formation of two covalent bonds in the insertion intermediate.

In the C–H activation of CH_4 by Mo, Siegbahn *et al.* have found that the insertion transition state and the ground state of $HMoCH_3$ have quintet spin multiplicity.[22] Similar results have also been calculated for the $Mo+H_2$ system.[31] Therefore, $Mo(^7S_3)$ encounters a large barrier to C–H bond insertion associated with promotion to the low-spin quintet surface. Such barriers may, in theory, be overcome by collision energy if the coupling between the surfaces is sufficiently strong. Since electronic energy has been observed to be efficient in promoting reaction, whereas collision energy is inefficient, we conclude that the crossing from the ground state septet surface onto the quintet surface is inefficient.

Spin–orbit coupling has been found to play an important role in a number of reactions involving transition metals. For Ni+CO, ground state $Ni(^3F_J)$ atoms were found to associate with CO with a relatively large third-order rate constant of $k=(6.9\pm0.5)\times10^{-32}\,cm^6\,s^{-1}$.[45] However, the ground state of NiCO is a $X\,^1\Sigma^+$ state, which correlates to $Ni(^1D_2)$ lying 3410 cm^{-1} above the ground state. Strong singlet–triplet coupling must lead to an adiabatic correlation between the ground state singlet NiCO complexes and the ground state $Ni(^3F_J)+CO(^1\Sigma^+)$ reactants in order to explain the observed association rate constant. Mitchell has carried out calculations to estimate the magnitude of the spin–orbit coupling between the $c\,^3\Pi$ and $X\,^1\Sigma^+$ surfaces for Ni+CO.[46] The crossing probability, P, for a single pass through the $c\,^3\Pi$ to $X\,^1\Sigma^+$ surface intersection was approximated by the Landau–Zener (LZ) equation (in the diatomic assumption)

$$P \approx 1-\exp\left[\frac{-4\cdot\pi^2\cdot M^2}{h\cdot F\cdot v_x}\right]. \tag{1}$$

In Eq. (1), M is the off-diagonal matrix element of the spin–orbit coupling operator, h is Planck's constant, F is the difference in gradients of the diabatic potential curves, and v_x is the relative velocity of the colliding partners. Approximating M as the spin–orbit coupling constant for the 3d electrons of Ni yielded a value for $P(^3\Pi \rightarrow {}^1\Sigma^+) > 0.99$ for a single pass through the curve crossing.[46] Even if the crossing is much less efficient than calculated, there still exists the possibility for multiple passes through the crossing region since both the $^3\Pi$ and the $^1\Sigma^+$ states of NiCO are bound. Thus, association of Ni(^3F_J) with CO($^1\Sigma^+$) to form NiCO($X\,^1\Sigma^+$) was found to follow an adiabatic pathway.

Another case where spin–orbit coupling appears to play an important role is in $Nb + C_2H_4 \rightarrow NbC_2H_2 + H_2$.[37] The ground state Nb atoms have a sextet spin multiplicity while C–H activation involves a quartet surface.[22] Deep potential wells associated with NbC_2H_4 association complexes exists on both the sextet and quartet surfaces.[47] It was found that Nb is efficiently able to access the quartet surface and proceed readily to form dehydrogenation products. Again, due to the deep wells, even if the crossing probability is low, the strongly bound long-lived high-spin complex allows for multiple crossings. This contrasts the $Mo + CH_4$ and $Mo + C_2H_6$ reactions, where the colliding partners only have one opportunity to cross onto the low-spin surface if insertion is to occur.

In $Ni + CO$ and $Nb + C_2H_4$, the high- and low-spin PESs are both strongly attractive, leading to similar gradients and a relatively small value of F, contributing to a large Landau–Zener crossing probability. Again, this contrasts the situation for $Mo + CH_4$ and $Mo + C_2H_6$. The crossings of the septet and quintet PESs for these systems are qualitatively analogous to that for $Mo + H_2$, where the $^7A_1$ surface is highly repulsive in the insertion (bending) coordinate, while the $^5B_2$ surface is highly attractive.[31] This leads to a large difference in the gradients for the two surfaces, thereby diminishing P. Additionally, it was found that spin–orbit coupling is not significant for $Mo + H_2$, resulting in a poor crossing efficiency in the LZ model.[31] It is interesting to note that in the analogous reaction involving W (lying directly below Mo in the periodic table), it was concluded that spin-orbit interactions were likely to be much more important.[48]

Finally, for collisions of Mo($^7S_3$) with C_2H_6, a high collision energy is required to overcome the insertion barrier. However, a large value for v_x in Eq. (1) will diminish the crossing probability. Armentrout *et al.* have studied the reactions of $Fe^+ + \text{propane}(C_3H_8)$ as a function of collision energy.[16] It was found that at low collision energies, below $E_{\text{coll}} \sim 0.5$ eV, the ground state $Fe^+(^6D)$ readily undergoes reaction, indicating that adiabatic crossing to a low-spin quartet surface is efficient at low collision energies. However, as the collision energy was increased, the dynamics were found to increasingly follow the diabatic pathway.[16]

It should be noted that the LZ model is based on a simple diatomic system with the crossing of only two PESs. For more complex systems such as $Mo + C_2H_6$, multiple PESs as well as a large number of internal degrees of freedom complicate this simple model. In any case, it is clear that the weak spin–orbit coupling between the septet and quintet surfaces, the large difference in the potential gradients, and high collision energy, combined with the direct nature of the insertion reaction, all contribute to the observed nonreactivity of the high-spin ground state of Mo($^7S_3$).

E. Absence of $MoCH_2$ and MoH_2 channels

As indicated in Fig. 1, the $Mo^*(^5S_2) + C_2H_6$ reaction may also lead to production of $MoH_2 + C_2H_4$. In a recent study of the reaction of ground state $Y + C_2H_6$,[33] both YH_2 and YC_2H_4 products were clearly observed from decay of $H_2YC_2H_4$ intermediates. In that case, formation of $YH_2 + C_2H_4$ was energetically only a few kcal/mol less favorable than formation of $YC_2H_4 + H_2$. Interestingly, the less thermodynamically favored $YH_2 + C_2H_4$ channel was actually found to be dominant, with the yield of YH_2 greater than YC_2H_4 by more than an order-of-magnitude. This indicated the existence of a potential energy barrier for H_2 elimination from $H_2YC_2H_4$ in excess of its thermodynamic threshold. The barrier for H_2 elimination is at least in part associated with the closed-shell s^2 character of Y in YC_2H_4.[33] For $Mo + C_2H_6$, on the other hand, the $MoC_2H_4 + H_2$ channel is favored by $\sim$ 15 kcal/mol relative to $MoH_2 + C_2H_4$. Furthermore, the Mo atom in MoC_2H_4 has substantial s^1 character and will therefore not interact repulsively with the dissociating H_2 fragment.[47] Consequently, elimination of H_2 from $H_2MoC_2H_4$ is expected to proceed through an essentially barrierless transition state. This is consistent with the $P(E)$ distributions which were always found to peak very close to zero kinetic energy. Thus, it is not surprising that the $Mo^*(^5S_2) + C_2H_6$ reaction leads exclusively to H_2 elimination.

The most thermodynamically favored products, $MoCH_2 + CH_4$, were not observed from $Mo^*(^5S_2) + C_2H_6$ even at the highest collision energy. From our studies of $Mo^*(^5S_2) + CH_4$ we know that $MoCH_2$ is readily detectable using 157 nm photoionization. Since the $MoCH_2 + CH_4$ channel is believed to result following C–C insertion, we conclude that C–C insertion is negligible for $Mo^*(^5S_2)$ over the range of collision energies studied in our experiment. Because the barrier height for C–C insertion into C_2H_6 lies considerably higher than that for C–H insertion,[22] and due to the less favorable steric factors for this process, it is perhaps not surprising that this channel is not observed. Interestingly, calculations indicate that in the $Mo + c\text{-}C_3H_6$ reaction, the barrier for C–C insertion is substantially lower than that for C–H insertion, offering the intriguing possibility that this process may actually be dominant at low collision energies for $Mo^*(^5S_2)$ reactions.[22]

V. CONCLUSIONS

The interactions of ground state Mo($^7S_3$) and metastable $Mo^*(^5S_2)$ atoms with CH_4 and C_2H_6 have been studied under single collision conditions. In the case of $Mo^*(^5S_2) + CH_4/C_2H_6$, dehydrogenation products ($MoCH_2/MoC_2H_4$) were the only observed products at every collision energy studied. For $Mo^*(^5S_2) + CH_4$, an upper limit of 2.1 kcal/mol (32.9 kcal/mol relative to $Mo(^7S_3) + CH_4$)) is placed on any

barriers along the reaction coordinate. *Ab initio* calculations have shown that all intermediates and barriers along the reaction coordinate to form dehydrogenation products are of quintet spin multiplicity, consistent with the observed reactivity of Mo*($^5S_2$). The $P(E_T)$s used to simulate the TOF spectra indicate that most of the available energy is channeled into product internal energy.

Nonreactive scattering of Mo($^7S_3$) was studied at a range in collision energies up to 14.4 kcal/mol for CH_4 and 35.4 kcal/mol for C_2H_6. The c.m. angular distribution found to best-fit the observed signal was identical to the $T(\Theta)$ used to fit Mo($^7S_3$)+Ar elastic scattering. These inelastic collisions were found to transfer 10% and 19% of the initial kinetic energy into internal energy of CH_4 and C_2H_6, respectively. Even at collision energies above the largest potential energy barrier for reaction with C_2H_6, ground state Mo($^7S_3$) atoms were unreactive, indicating that translational energy is ineffective in promoting C–H bond activation.

ACKNOWLEDGMENTS

This work was supported by the National Science Foundation. Some of the equipment used in this study was funded by an NSF Faculty Early Career Development Award, an NSF equipment grant, and by an ONR Young Investigator Award. Additional support from the Exxon Educational Foundation is also gratefully appreciated. R. Z. H. would like to thank the Department of Education for a Graduate Fellowship. H.U.S. thanks the Link Foundation and Procter & Gamble for Graduate Fellowships. The authors would like to thank J. Weisshaar for valuable discussions and suggestions.

[1] R. H. Crabtree, *The Organometallic Chemistry of the Transition Metals* (Wiley, New York, 1994).
[2] M. J. Burk and R. H. Crabtree, J. Am. Chem. Soc. **109**, 8025 (1987).
[3] A. H. Janowicz and R. G. Bergman, J. Am. Chem. Soc. **104**, 352 (1982).
[4] R. G. Bergman, Science **223**, 902 (1984).
[5] E. P. Wasserman, C. B. Moore, and R. G. Bergman, Science **255**, 315 (1992).
[6] A. A. Bengali, R. G. Bergman, and C. B. Moore, J. Am. Chem. Soc. **117**, 3879 (1995).
[7] P. E. M. Siegbahn, J. Am. Chem. Soc. **118**, 1487 (1996).
[8] W. E. Billups, M. M. Konarski, R. H. Hauge, and J. L. Margrave, J. Am. Chem. Soc. **102**, 7393 (1980).
[9] G. A. Ozin, D. F. McIntosh, S. A. Mitchell, and J. García-Prieto, J. Am. Chem. Soc. **103**, 1574 (1981).
[10] J. M. Parnis and G. A. Ozin, J. Phys. Chem. **93**, 4023 (1989).
[11] A. J. Rest, I. Whitwell, W. A. G. Graham, J. K. Hoyano, and A. D. McMaster, J. Chem. Soc., Chem. Commun. **1984**, 624.
[12] R. L. Rubinovitz and E. R. Nixon, J. Phys. Chem. **90**, 1940 (1986).
[13] P. B. Armentrout, Annu. Rev. Phys. Chem. **41**, 313 (1990).
[14] J. C. Weisshaar, Adv. Chem. Phys. **82**, 213 (1992).
[15] P. E. M. Siegbahn and M. R. A. Blomberg, J. Am. Chem. Soc. **114**, 10548 (1992).
[16] R. H. Schultz, J. L. Elkind, and P. B. Armentrout, J. Am. Chem. Soc. **110**, 411 (1988).
[17] M. A. Tolbert and J. L. Beauchamp, J. Am. Chem. Soc. **106**, 8117 (1984).
[18] J. L. Elkind and P. B. Armentrout, J. Phys. Chem. **91**, 2037 (1987).
[19] L. Sunderlin, N. Aristov, and P. B. Armentrout, J. Am. Chem. Soc. **109**, 78 (1987).
[20] N. Aristov and P. B. Armentrout, J. Am. Chem. Soc. **108**, 1806 (1986).
[21] J. J. Carroll, K. L. Haug, and J. C. Weisshaar, J. Am. Chem. Soc. **115**, 6962 (1993).
[22] J. J. Carroll, K. L. Haug, J. C. Weisshaar, M. R. A. Blomberg, P. E. M. Siegbahn, and M. Svensson, J. Phys. Chem. **99**, 13955 (1995).
[23] K. Honma, Phys. Chem. Chem. Phys. **1**, 3235 (1999).
[24] L. Lian, S. A. Mitchell, and D. M. Rayner, J. Phys. Chem. **98**, 11637 (1994).
[25] Y. Wen, A. Yethiraj, and J. C. Weisshaar, J. Chem. Phys. **106**, 5509 (1997).
[26] Y. Wen, J. Rau, M. Porembski, and J. C. Weisshaar, Abstract in Dynamics of Molecular Collisions Conference XVI, Brainerd, Minnesota (1997).
[27] P. A. Willis, H. U. Stauffer, R. Z. Hinrichs, and H. F. Davis, J. Chem. Phys. **108**, 2665 (1998).
[28] P. E. M. Siegbahn, J. Am. Chem. Soc. **115**, 5803 (1993). These calculations were performed at a different level of theory compared to Ref. 22. The values were adjusted by matching the energetics of the $Mo(H)_2C_2H_4$ complex.
[29] J. Berkowitz, G. B. Ellison, and D. Gutman, J. Phys. Chem. **98**, 2744 (1994).
[30] C. E. Moore, *Atomic Energy Levels* (National Bureau of Standards, Washington, D.C., 1952).
[31] J. Li and K. Balasubramanian, J. Phys. Chem. **94**, 545 (1990).
[32] P. E. M. Siegbahn, Theor. Chim. Acta **87**, 441 (1994).
[33] H. U. Stauffer, R. Z. Hinrichs, J. J. Schroden, and H. F. Davis, J. Phys. Chem. A. (in press).
[34] P. A. Willis, H. U. Stauffer, R. Z. Hinrichs, and H. F. Davis, Rev. Sci. Instrum. **70**, 2606 (1999).
[35] C. H. Corliss and W. R. Bozman, Experimental Transition Probabilities (National Bureau of Standards, Washington, D.C., 1962).
[36] *C.R.C. Handbook of Chemistry and Physics*, 75th ed., edited by D. R. Lide (CRC, Boca Raton, FL, 1994).
[37] P. A. Willis, H. U. Stauffer, R. Z. Hinrichs, and H. F. Davis, J. Phys. Chem. A **103**, 3706 (1999).
[38] H. U. Stauffer, R. Z. Hinrichs, P. A. Willis, and H. F. Davis, J. Chem. Phys. **111**, 4101 (1999).
[39] J. M. Parson, T. P. Schafer, F. P. Tully, P. E. Siska, Y. C. Wong, and Y. T. Lee, J. Chem. Phys. **53**, 2123 (1970).
[40] U. Buck, J. Schleusener, D. J. Malik, and D. Secrest, J. Chem. Phys. **74**, 1707 (1981).
[41] I. Wallace and W. H. Breckenridge, J. Chem. Phys. **97**, 2318 (1992).
[42] P. A. Willis, Ph.D. Thesis, Cornell University, 1999.
[43] H. U. Stauffer, R. Z. Hinrichs, J. J. Schroden, and H. F. Davis, J. Chem. Phys. **111**, 10758 (1999).
[44] N. Koga, S. Obara, K. Kitaura, and K. Morokuma, J. Am. Chem. Soc. **107**, 7109 (1985).
[45] C. E. Brown, S. A. Mitchell, and P. A. Hackett, Chem. Phys. Lett. **191**, 175 (1992).
[46] S. A. Mitchell, in *Gas-Phase Metal Reactions*, edited by A. Fontijn (North-Holland, Amsterdam, 1992), Chap. 12.
[47] M. R. A. Blomberg, P. E. M. Siegbahn, and M. Svensson, J. Phys. Chem. **96**, 9794 (1992).
[48] K. Balasubramanian and Z. Ma, J. Phys. Chem. **95**, 9794 (1991).